Study of Detonation in Isopropyl Nitrate-Air Mixtures

Xiangrong Huang[1], Vigneshwaran Sankar[2,3], Karl P. Chatelain[2,3],
Rémy Mével[4], Deanna A. Lacoste[2,3]
[1]School of Aerospace Engineering, Tsinghua University, Beijing, China
[2]Mechanical Engineering Program, Physical Science and Engineering Division, King Abdullah University of Science and Technology (KAUST), Thuwal 23955-6900, Saudi Arabia
[3]Clean Energy Research Platform (CERP), King Abdullah University of Science and Technology of Science and Technology (KAUST), Thuwal, 23955-6900, Saudi Arabia
[4]School of Aeronautics and Astronautics, Zhejiang University, Hangzhou, China

1 Introduction

The exothermic decomposition and combustion properties of isopropyl nitrate ($iC_3H_7ONO_2$, IPN) has motivated its utilization as a gas generator and monopropellant in rocket engineering [1]. IPN may also serve as an additive to fuels in diesel engines [2,3]. Decomposition of IPN begins with the rupture of the weak O-NO_2 bond, $iC_3H_7ONO_2$=iC_3H_7O+NO_2, which is followed by β-scission, iC_3H_7O=CH_3CHO+CH_3 or by H-elimination iC_3H_7O=CH_3COCH_3+H (minor pathway) [4]. Such a process produces NO_2, H, and CH_3 radicals, which promote ignition and subsequent combustion [3]. Zhang et al. [5] explored the sensitization effect of gaseous IPN on the detonation of hydrocarbon-air mixtures, and investigated the initiation and detonability of liquid IPN [6]. Ignition delay-times of gaseous IPN-O_2-Ar mixtures were measured by [3]. Recently, Fuller et al. [4] proposed a detailed IPN mechanism, and measured the flame speed and ignition delay-time for IPN-propane-air mixtures [7]. In the current study, the cellular detonation structure of gaseous IPN-air mixtures has been investigated numerically.

a) ϕ=1 ; P_1=10 kPa b) ϕ=1 ; P_1=100 kPa c) ϕ=0.7 ; P_1=100 kPa

Figure 1: Soot foils obtained for IPN-air mixtures under various conditions.

2 Recallection of the experimental results

The detonation structure of IPN-air mixtures was studied by [8]. Two series of experiments were conducted: (i) stoichiometric, $\phi = 1$, IPN-air mixtures initially at 10-100 kPa; and (ii) ϕ =0.4-3 IPN-air mixtures initially at P_1=100 kPa and T_1 up to 386 K. For further details about the experiments, see [8].

Figure 1 shows the soot foils recorded under three typical conditions, while the measured cell sizes are shown in Fig. 2, along with the induction length computed with the ZND model. In Fig. 2, red squares

represent the average cell size (λ), while the error bars indicate the range of observed cell width in the soot foil. The ratio between maximum and minimum cell width varies from 1.3 to 2.0. The experimental conditions and results are listed in Table 1. For the P_1=10 kPa case, the shock tends to be overdriven, with a relative error between the measured and the calculated CJ speed close to 3%.

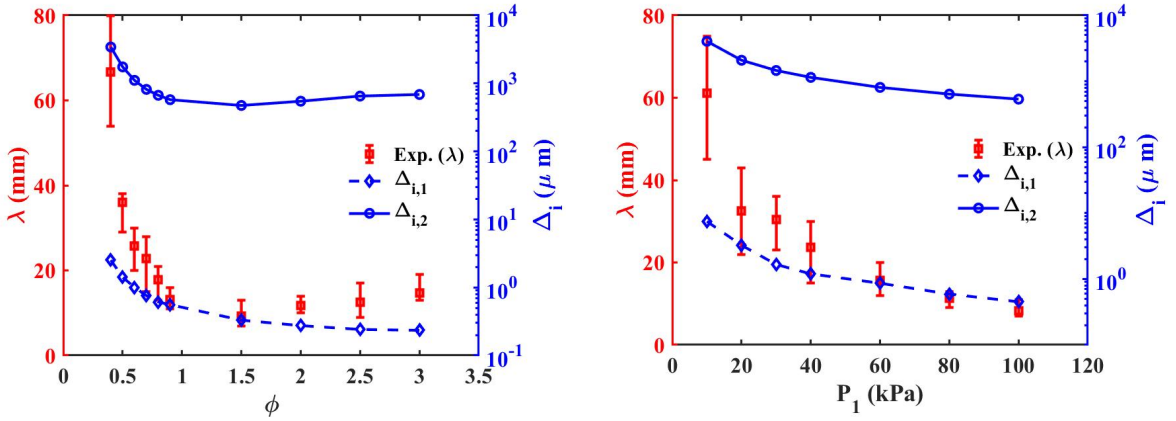

Figure 2: Measured cell size and simulated induction length. Simulations were done with the ZND model using SDToolbox. Error bars indicate the range of observed cell width.

Table 1: Experimental conditions and measured cell width (λ). *: calculated based on ZND model and detailed mechanism [4]. Induction length is defined as the distance to temperature gradient peaks.

P_1 (kPa)	T_1 (K)	ϕ	λ (mm)	$\lambda_{\min}$ (mm)	$\lambda_{\max}$ (mm)	D_{meas} (m/s)	D^*_{CJ} (m/s)	diff. (%)	$\Delta^*_{i,1}$ (μm)	$\Delta^*_{i,2}$ (mm)	$\frac{\lambda}{\Delta_{i,1}}$	$\frac{\lambda}{\Delta_{i,2}}$	$\frac{\Delta_{i,2}}{\Delta_{i,1}}$
10	374	1	61.08	45	75	1855.0	1800.3	3.04	7.47	4.05	8171	15.09	541
20	365	1	32.6	22	43	1776.3	1817.6	-2.27	3.25	2.09	10036	15.61	643
30	299	1	30.5	23	36	1796.2	1833.4	-2.03	1.66	1.46	18365	20.91	878
40	299	1	23.7	15	30	1820.1	1839.8	-1.07	1.20	1.15	19827	20.65	960
60	357	1	15.7	12	20	1822.0	1843.4	-1.16	0.86	0.81	18211	19.42	938
80	358	1	11.3	9	13	1818.3	1849.7	-1.70	0.59	0.64	19126	17.66	1083
100	349	1	8.2	7	11	1869.1	1855.4	0.74	0.45	0.54	18184	15.28	1190
100	372	0.4	66.7	54	80	1501.8	1521.5	-1.29	2.53	3.43	26409	19.45	1358
100	376	0.5	36	29	38	1615.8	1619.7	-0.24	1.42	1.75	25436	20.58	1236
100	376	0.6	25.7	20	30	1689.9	1693.2	-0.19	1.00	1.11	25632	23.15	1107
100	377	0.7	22.75	15	28	1737.7	1748.5	-0.61	0.76	0.82	30017	27.83	1079
100	372	0.8	17.8	13	21	1774.6	1791.4	-0.94	0.61	0.67	29050	26.59	1093
100	386	0.9	13.2	11	16	1810.3	1824.6	-0.78	0.56	0.58	23669	22.89	1034
100	377	1.5	9.2	7	13	1931.8	1938.7	-0.36	0.33	0.47	27856	19.40	1436
100	385	2	11.8	10	14	1961.6	1974.9	-0.67	0.27	0.55	42960	21.55	1993
100	374	2.5	12.5	9	17	1965.9	1989.6	-1.19	0.24	0.65	51804	19.18	2700
100	378	3	14.7	13	19	1986.0	1996.2	-0.51	0.23	0.69	62742	21.38	2935

3 Steady structure analysis

The detailed IPN kinetic mechanism recently developed by Fuller et al. [4] was adopted to analyze the steady detonation structure computed with the ZND solver in the SDToolbox [9]. Typically, the ZND solutions for IPN-air mixtures have two stages of energy release, see Fig. 3. Therefore, two induction lengths were defined as the distances to temperature gradient peaks, shown as the black dashed lines in

Fig. 3. The mole fraction profiles of major species are also presented: (i) the IPN concentration rapidly decays around the peak of heat release; (ii) the concentration of N radical is not significant until the first peak of energy release; (iii) the profile of the H radical is well correlated with the temperature profile; (iv) the NO concentration remains high throughout the entire ZND structure; (v) the mole fractions of NO_2 and CH_3 reach maximum at the first induction length, and decays steeply after the second induction length. The calculated induction length is presented as in Fig. 2 and Table 1. Both $\Delta_{i,1}$ and $\Delta_{i,2}$ decrease monotonically as P_1 increases. As ϕ increases, $\Delta_{i,1}$ decreases monotonically, while $\Delta_{i,2}$ demonstrates a minimum around ϕ=1.5. The monotonic decrease of $\Delta_{i,1}$ with ϕ may be explained by the increase of the post-shock pressure at the von Neumann state. This speeds up the dissociation of IPN, $iC_3H_7ONO_2$=iC_3H_7O+NO_2, which leads to the formation of important amounts of reactive species. The minimum value of $\Delta_{i,2}$ is located on the rich side, ϕ=1.5.

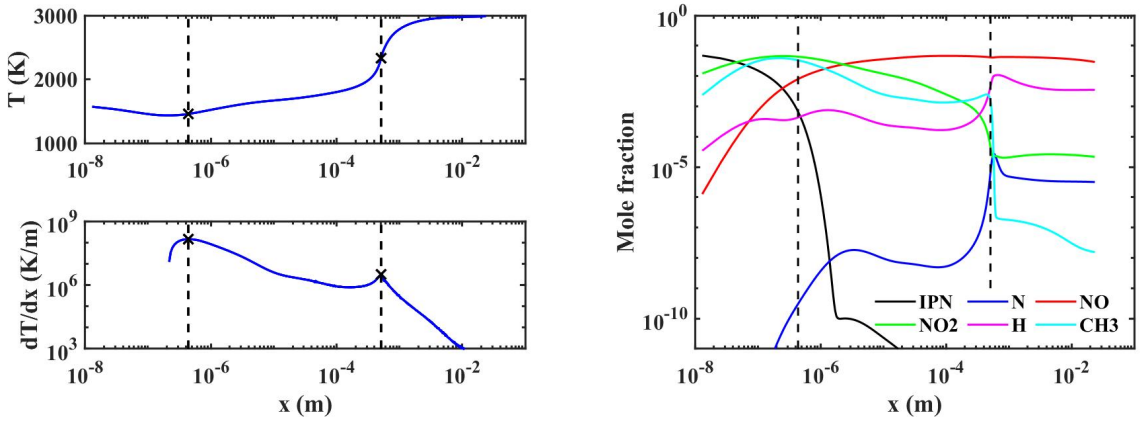

Figure 3: Temperature and temperature gradient profiles (left), and mole fraction profiles (right). Calculated with ZND model for stoichiometric IPN-air mixture initially at 376 K and 100 kPa. Black dashed lines indicate the induction lengths, which are defined with the peaks of temperature gradient.

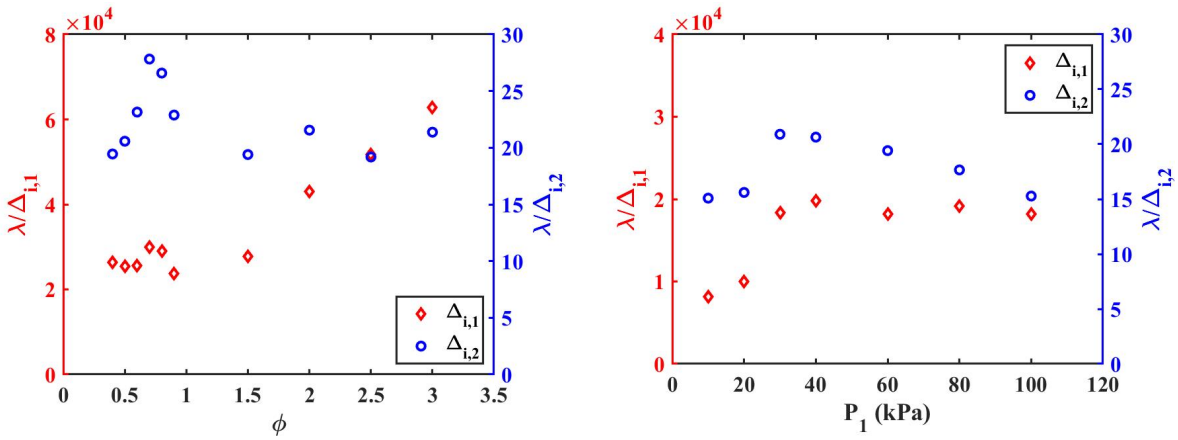

Figure 4: Ratio of cell size and induction length for various ϕ (left), and P_1 (right).

Multi-stage of energy release potentially leads to the double cellular structure, as observed in fuel-NO_2/N_2O_4 mixtures [10]. In the current IPN-air experiments, the double cellular structure was not captured by the soot foils, despite the pronounced two steps of heat release. Therefore, it is relevant to briefly review the characteristics of the ZND structures previously computed for fuel-NO_2/N_2O_4 mixtures. Joubert et al. [10] indicated that H_2-NO_2/N_2O_4 mixtures demonstrate two steps of energy release, induced by the reaction NO_2+H=NO+OH and the oxidization of NO, respectively. For fuel-

NO_2/N_2O_4 mixtures initially at 1-2 bar, the double cellular structure exists only when $\phi > 1$. When P_1=100 kPa, the ratio between $\lambda_1/\Delta_{i,1} \approx$ 20, 10, 25 when the fuel is H_2, CH_4 or C_2H_6, repetitively, while $\lambda_2/\Delta_{i,2} \approx$ 15, 30 or 50. This range of ratio is consistent with [11], where values in the range 10∼100 were indicated. Furthermore, $\Delta_{i,2}/\Delta_{i,1} \approx$ 7∼100 for H_2-NO_2/N_2O_4 mixtures. According to Table 1 and Fig. 4, there is a significant difference between the magnitude of the two induction lengths for IPN-air mixtures, i.e., $\Delta_{i,1} \sim \mathcal{O}(1\ \mu\text{m})$ while $\Delta_{i,2} \sim \mathcal{O}(1\text{ mm})$, resulting in $\Delta_{i,2}/\Delta_{i,1} \approx$ 541∼2935. The ratio of cell width to induction length is $\lambda/\Delta_{i,2} \approx$15∼28, which is a reasonable range and is consistent with [10, 11]. Adopting the range (10∼100) from [11], we might expect a maximum cell size of λ_1=0.75 mm corresponding to the first step of energy release. Such small features would be difficult to capture experimentally, which could explain why a double cellular structure was not observed.

4 Chemical analysis

We first identify the controlling reactions for both steps of energy release through a heat release rate (HRR) analysis. Second, we perform brute-force sensitivity analyses to determine the dominant reactions for each step of heat release.

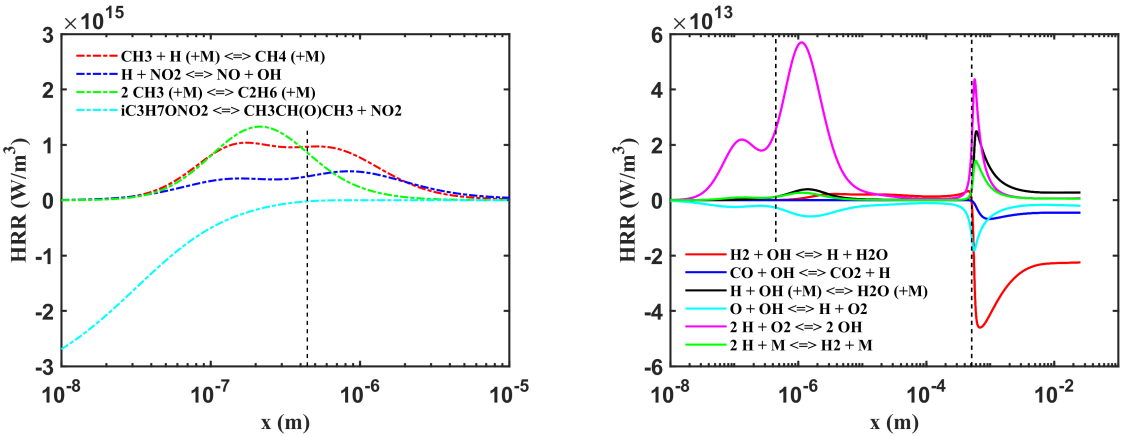

Figure 5: Heat release rate (HRR) profile around the first induction length (left), and profile for the whole ZND structure (right). Calculated with ZND model for stoichiometric IPN-air mixture initially at 376 K and 100 kPa. Black dashed lines indicate the induction length. Reactions illustrated in the left figure are not shown in the right figure, since their integrated contributions to the total energy release are minor.

4.1 Heat release rate analysis

Heat release rate analysis was conducted to identify the dominant reactions for both stages of energy release in the ZND solution. Figure 5 illustrates the HRR profiles for a IPN-air mixture initially at 376 K and 100 kPa. The dissociation of IPN is the main endothermic reaction, whereas the recombination reactions for CH_3 and chain initiation reaction H+NO_2=NO+OH provide the heat for the first step of temperature increase. This feature is correlated with the peaks of mole fraction for NO_2 and CH_3 around the end of $\Delta_{i,1}$. NO_2 mainly originates from the dissociation of IPN, $iC_3H_7ONO_2$=iC_3H_7O+NO_2, while CH_3 comes from the subsequent β-scission, iC_3H_7O=CH_3CHO+CH_3. These dominant processes were also identified under other conditions, i.e., for P_1=100 kPa and ϕ=0.4-3 and for P_1=10-100 kPa and ϕ=1. The right subfigure of Fig. 5 illustrates the controlling reactions for the second stage of energy

release. Reaction H_2+OH=H+H_2O and O+OH=H+O_2 are the two main endothermic reactions for various initial conditions. For mixtures with ϕ=0.4-1, and at P_1=10-100 kPa, the dominant exothermic reactions are mainly from the H/O chemical system, i.e., 2H+O_2=2OH, as well as the recombination reactions of H and OH radicals. For rich mixtures (ϕ=1-3, P_1=100 kPa), CH_3+H(+M)=CH_4(+M) and CH_4+H=CH_3+H_2 instead of H/O reactions contribute mainly to the energy release.

4.2 Sensitivity analysis

Sensitivity analyses were performed for stoichiometric IPN-air mixtures initially at T_1=373 K and P_1=10, 100 kPa, see Fig. 6. Sensitivity coefficients of one specific reaction, c_i, were calculated with the brute forced approach,

$$c = \frac{d \ln \Delta_i}{d \ln k} \approx \frac{\ln \Delta_i^{'} - \ln \Delta_i}{\ln k^{'} - \ln k}, \tag{1}$$

where Δ_i was calculated with rate constant k, while $\Delta_i^{'}$ was obtained when perturbing $k^{'} = 1.1k$. For the $\Delta_{i,1}$, IPN dissociation reaction and recombination of CH_3 have dominating effects, while reaction CH_3+NO_2=CH_3O+NO is essential only under low-pressure conditions. As for $\Delta_{i,2}$, a number of reactions have significant effects. Among them, the reaction O+OH=H+O_2 is found to be the dominant one.

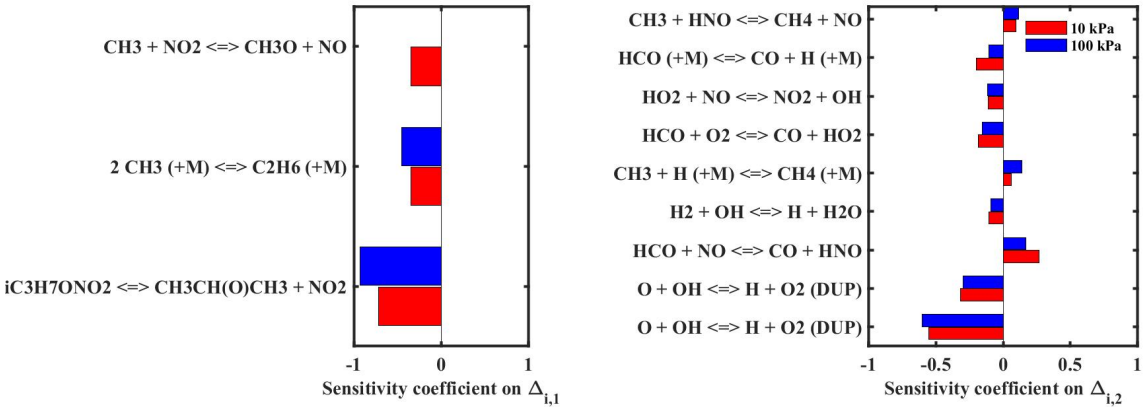

Figure 6: Sensitivity coefficients for both induction length, $\Delta_{i,1}$ (left) and $\Delta_{i,2}$ (right). Analysis was done for stoichiometric IPN-air mixtures initially at T_1=373 K, and P_1=10 (red), and 100 (blue) kPa.

5 Conclusion

In the current study, the ZND structure of IPN-air mixtures was studied for mixtures with ϕ=0.4-3 and initially at T_1 up to 386 K, P_1=10-100 kPa. IPN-air mixtures demonstrate two induction lengths within the ZND solution, which might potentially lead to a double cellular structure, as in rich fuel-NO_2/N_2O_4 mixtures. Currently, no double structure could be identified in the experimental soot foils, which is attributed to the very small size of the potential small cellular network (λ <0.75 mm). In the future study, 2D simulations will be conducted to explore if the assumed double cellular structure could be identified numerically. This will be a challenging work due to the significant ratio between the characteristic length scales of the two stages of energy release, i.e., $\Delta_{i,2}/\Delta_{i,1}$. Namely, it is extremely computationally expensive to resolve both induction lengths in a 2D simulations.

Acknowledgments

The experiments were performed at Caltech and presented at the 2007 Fall Technical Meeting of the Western States Sections of the Combustion Institute, see [8]. The authors are grateful to Dr James Karnesky and Prof Joseph E. Shepherd for providing additional data from their study, such as some soot foils.

References

[1] Griffiths JF, Gilligan MF, Gray P (1975), Pyrolysis of isopropyl nitrate. I. Decomposition at low temperatures and pressures. Combustion and flame 24: 11-19.

[2] Hansson T, Pettersson JBC, Holmlid L (1989). A molecular beam mass-spectrometric study of isopropyl nitrate pyrolysis reactions at short residence times and temperatures up to 700 K. Journal of the Chemical Society, Faraday Transaction 2 85 (9): 1413-1423.

[3] Toland A, Simmie JM (2003). Ignition of alkyl nitrate/oxygen/argon mixtures in shock waves and comparisons with alkanes and amines. Combustion and flame 132: 556-564.

[4] Fuller ME, Goldsmith CF (2019). Shock tube laser schlieren study of the pyrolysis of isopropyl nitrate. The Journal of Physical Chemistry A 123: 5866-5876.

[5] Zhang F, Akbar R, Thibault PA, Murray SB (2001). Effects of nitrates on hydrocarbon-air flames and detonations. Shock Waves 10: 457-466.

[6] Zhang F, Yoshinaka A, Murray SB, Higgins A (2002). Shock initiation and detonability of isopropyl nitrate. In 12th International Detonation Symposium, ONR 335-05-2.

[7] Fuller ME, Mousse-Rayaleh A, Chaumeix N, Goldsmith FC (2022). Laminar flame speeds and ignition delay times for isopropyl nitrate and propane blends. Combustion and Flame 242: #112187.

[8] Karnesky J, Pitz WJ, Shepherd JE (2007). Detonation in gaseous isopropyl nitrate mixtures. In WSSCI 2007 Fall Technical Meeting, #07F-40. `https://shepherd.caltech.edu/EDL/publications/reprints/ipn_wssci07.pdf`.

[9] Shock and Detonation Toolbox (2021 Version, updated 11-Feb-2023), `https://shepherd.caltech.edu/EDL/PublicResources/sdt//index.html`.

[10] Joubert F, Desbordes D, Presles H-N (2008). Detonation cellular structure in NO_2/N_2O_4–fuel gaseous mixtures. Combustion and Flame 152: 482-495.

[11] Akbar R, Kaneshige M, Shepherd JE (1997). Detonations in H_2-N_2O-CH_4-NH_3-O_2-N_2 mixtures. In GALCIT Technical Report FM97-3. `https://shepherd.caltech.edu/EDL/publications/r_akba97b/rep3.pdf`.